A Comparison between Observed and GCM-Simulated Summer Monsoon Characteristics over China

ARTHUR N. SAMEL

Atmospheric Sciences Research Center, State University of New York at Albany, Albany, New York

SHAOWU WANG

Department of Geosciences, Beijing University, Beijing, China

WEI-CHYUNG WANG

Atmospheric Sciences Research Center, State University of New York at Albany, Albany, New York

22 June 1994 and 12 December 1994

ABSTRACT

Observed rainfall over China and sea level pressure over Eurasia, two parameters that are closely associated with the east Asian summer monsoon, are compared with those simulated in a general circulation model (GCM). Observations are for the period 1951–1990 and include two datasets: a 160-station rainfall archive for China and a gridded sea level pressure record for Eurasia. The GCM dataset contains output from a 40-yr simulation with a mixed-layer ocean and greenhouse gas concentrations prescribed at 1990 levels.

In both observations and the model simulation, empirical orthogonal function (EOF) analysis identifies two rainfall regions, the Yangtze River valley and southeast China, where interannual variability is large but relatively homogeneous. The locations of the model regions, however, are systematically shifted several degrees to the west. For each observed and model region, area-averaged summer rainfall anomalies are used to develop a 40-yr intensity index time series. Correlations between the regional indices and sea level pressure indicate that intensity values are influenced by the interaction of several circulation features. Observed rainfall intensifies over the Yangtze River valley when interactions between the Siberian high, subtropical high, and monsoon low cause the temperature gradient across the Mei-Yu front to increase. These interactions are accurately reproduced in the model simulation. Observed intensity over southeast China increases when the monsoon low moves to the north while GCM rainfall intensifies when the monsoon low deepens over southeast China and sea level pressure increases over the Tibetan Plateau.

1. Introduction

The climate of China is strongly influenced by the east Asian monsoon. The primary physical manifestation of the summer monsoon is heavy precipitation. The summer rainfall pattern over China is determined by the configuration of the Eurasian circulation, which shows several distinct features. These include the monsoon low over south-central Asia, the subtropical high over the west-central Pacific Ocean, the Mei-Yu front along the Yangtze River valley, and the Siberian high over south-central Siberia (Tao and Chen 1987; Liang et al. 1994a; Fig. 1a). Observed summer rainfall over China is heaviest over the south and, in general, decreases to the north (Fig. 1b; Legates and Wilmott 1990). In addition, rainfall anomalies undergo substantial interannual variability that results from changes in the location and strength of the Eurasian circulation features listed above (Fu et al. 1986; Wang and Li 1990; Zhu and Li 1992; Liang et al. 1994a).

General circulation models (GCMs), partly because of their coarse horizontal grid resolutions, cannot reproduce aspects of the rainfall field that have a high degree of spatial variability (Giorgi 1990; Hurrell et al. 1993). Nor can they simulate observed intraseasonal changes in these smaller-scale precipitation patterns (Tibaldi et al. 1990). Sperber et al. (1994) found that model simulations of monthly rainfall over China during the summer become more detailed and accurate as horizontal grid resolution increases. Hence, when the GCM grid is coarse, comparisons between observed and model-generated rainfall anomalies are more meaningful when seasonal, rather than monthly, values are considered.

To date, no study has investigated the ability of a coarse-resolution GCM to reproduce regional interannual variations in summer rainfall over east Asia. Hence, the purpose of this note is to develop a descrip-

Corresponding author address: Dr. Arthur N. Samel, ASRC/SUNY, 100 Fuller Road, Albany, NY 12205.

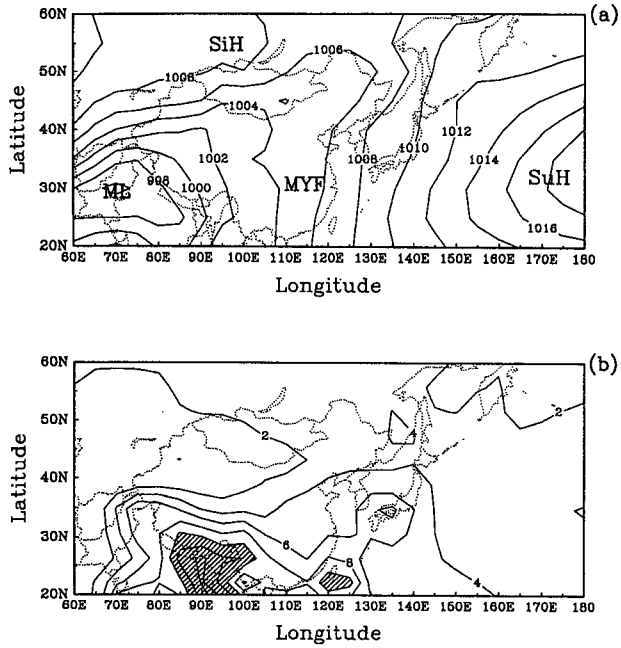

FIG. 1. Mean summer (June, July, August) sea level pressure (in millibars) over Eurasia and adjacent oceanic areas for 1951–1990 (a). The locations of the monsoon low, Siberian high, subtropical high, and Mei-Yu front are indicated by ML, SiH, SuH, and MYF, respectively. Average observed summer rainfall distribution (in mm day^{-1}) over China and adjacent areas (b).

tion of the east Asian summer monsoon over China and to compare observed features with those from a GCM simulation of the present climate. Rainfall regions are initially identified, where anomaly interannual variability within a specific region is large but relatively homogeneous. Relationships between interannual variability in regional anomalies and the Eurasian sea level circulation are then determined.

The observed and GCM data used in this study are described in section 2. Observed and GCM-simulated east Asian monsoon characteristics are identified and compared in section 3. Concluding remarks are given in section 4.

2. Observed data and the model simulation

Two 40-yr observed datasets are used to study east Asian summer monsoon characteristics. The 160-station rainfall record for China contains monthly values for the period January 1951 to December 1988 (Tao et al. 1991). Additional data for the period January 1989 through December 1990 were obtained from the Central Meteorological Service of the Chinese Meteorological Administration. For each station, yearly summer rainfall is defined to be the June, July, August (JJA) total, where anomalies are given as deviations from the 40-yr JJA station mean. Monthly sea level pressure data from January 1951 to December 1990 are provided for a 5° lat × 5° long grid that extends from 20° to 90°N and 180°E to 180°W (Jenne 1989). The gridpoint anomaly for a specific summer is defined to be the difference between the June, July, August (JJA) average and the 40-yr JJA mean.

The GCM data come from the first 40 yr of a 100-yr National Center for Atmospheric Research CCM1 simulation of the present climate, as described by Wang et al. (1992). A 40-yr period is chosen to match the length of the observed datasets. The model contains a bulk land surface, a mixed layer ocean, and an atmosphere with 12 vertical levels where the horizontal resolution is R15; approximately 4.5° lat × 7.5° long. Surface variables such as temperature, snow cover, sea ice, and sea surface temperature are predicted by the model. Although the topography in an R15 resolution model is unrealistic and the mixed layer ocean does not generate sufficient interannual variability in tropical sea surface temperatures, simulated means and interannual variations over east Asia and adjacent oceanic regions are in general agreement with observed values (detailed descriptions are given in Liang et al. 1994a and 1994b).

For each grid cell, simulated summer rainfall and sea level pressure anomalies are defined as in observations and are analyzed over a domain that extends from 20°N to 70°N and 60°E to 180°E. Analysis of the GCM mean summer sea level pressure field (Fig. 2a) indicates that the model reproduces the fundamental features of the observed Eurasian circulation (Fig. 1a). The model monsoon low, however, has a much lower central pressure and is located approxi-

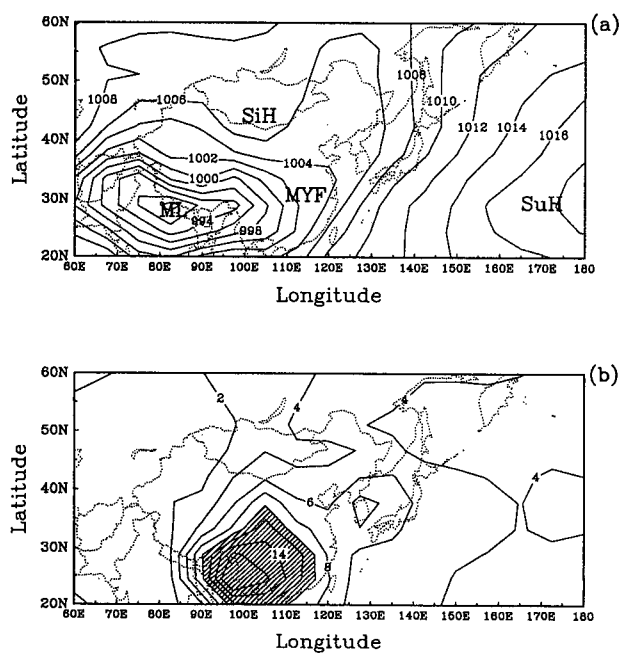

FIG. 2. Same as Fig. 1 except for years 1–40 of the GCM simulation.

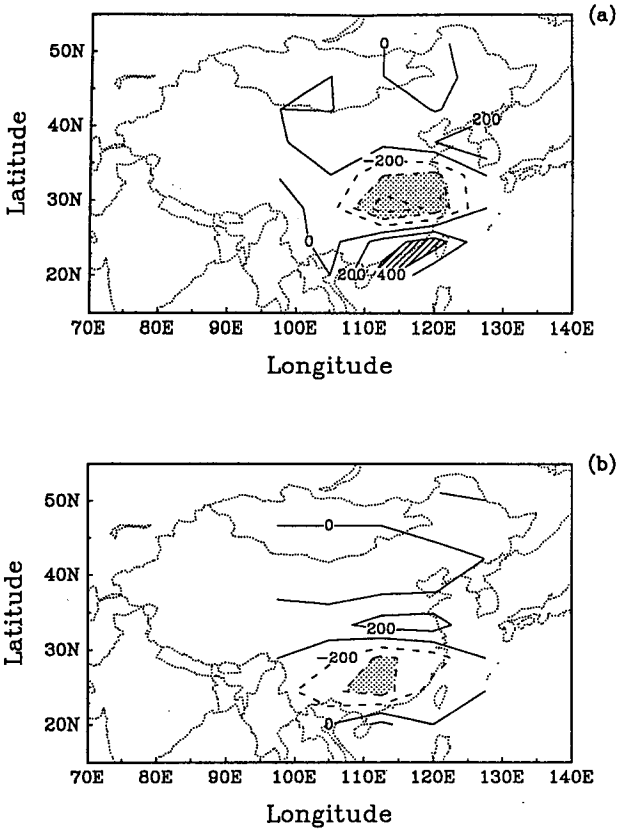

FIG. 3. Loading pattern in observed EOFs 1 (a) and 2 (b). The contour interval is 200 units where dashed contours indicate negative values. Hatched areas correspond to loadings greater than 400, while stippling indicates values less than −400. Note that loading values are interpolated to the GCM horizontal grid.

mately one grid point to the east of the observed feature. Furthermore, the inverted ridge identified with the Siberian high has a larger amplitude in the simulation. Thus, the GCM sea level pressure gradient over China is larger than observations. General features of the observed summer precipitation pattern over China are also simulated by the model (Fig. 2b), where rainfall rates decrease from south to north. GCM precipitation in most of China is, however, heavier than observations. In addition, while the largest observed rates are oriented along an east–west axis, the model maximum is circular and centered over the China–Burma border.

3. East Asian summer monsoon characteristics

The observed summer rainfall anomaly pattern in China is the result of important intraseasonal variations that occur in the detailed structure of the precipitation field (Lau and Li 1984; Tao and Chen 1987; Lau et al. 1988). In general terms, monsoon rainfall moves from south to north in a stepwise manner. Precipitation arrives along the south China coast during mid May and remains over south China until the beginning of June. At this time, rainfall abruptly shifts to the Yangtze River valley and is located along the Mei-Yu front through the first 10 days of July. The precipitation then advances to the north and persists over north China through the first 10 days of August. Monsoon rainfall then retreats quickly to the south during the second half of August and September. The low-level circulation over east Asia changes from being cyclonic to anticyclonic and, as a result, precipitation over China is greatly decreased.

The above climatology outlines the stepwise advance and retreat of the summer monsoon in China. There exist, however, large interannual variations in rainfall duration and intensity. Hence, anomaly interannual variability is likely to be focused over three "rainfall" regions: north China, the Yangtze River valley, and south China. Empirical orthogonal function (EOF) analysis is applied to the 160-station rainfall anomaly dataset to determine whether variability is maximized over these regions. The analysis produces an ordered set of unrotated EOFs, where each successive EOF explains a smaller fraction of total field variance. When the loadings of each EOF are mapped, the regions with the largest values correspond to the locations where anomaly interannual variability is large but relatively homogeneous. Note that only EOF1 and EOF2 are considered in this study because the phase and magnitude of higher-order loading patterns are found to be highly sensitive to changes in the spatial data domain.

The loading pattern of EOF1 (Fig. 3a) indicates that anomaly interannual variability is centered over the Yangtze River valley and southeast China. In EOF2 (Fig. 3b), the Yangtze River valley is the boundary between centers to the north and south. Total rainfall anomaly variance explained by EOF1 and EOF2 is 12.2% and 8.1%, respectively. The lack of a well-defined loading center over north China in both EOF1 and EOF2 indicates that anomaly interannual variability is not focused over this region. Hence, there exist two coherent regions in east China (hereafter called rainfall regions) where observed interannual variability is large: the Yangtze River valley and southeast China (Table 1).

TABLE 1. Observed and GCM rainfall regions. Anomaly interannual variability within each region is large and relatively homogeneous.

Region	Observed domain	GCM domain
Yangtze River valley	30°–34°N, 114°–120°N	26.7°–35.6°N, 101.25°–116.25°E
Southeast China	23°–26°N, 111°–119°E	17.8°–26.7°N, 101.25°–116.25°E

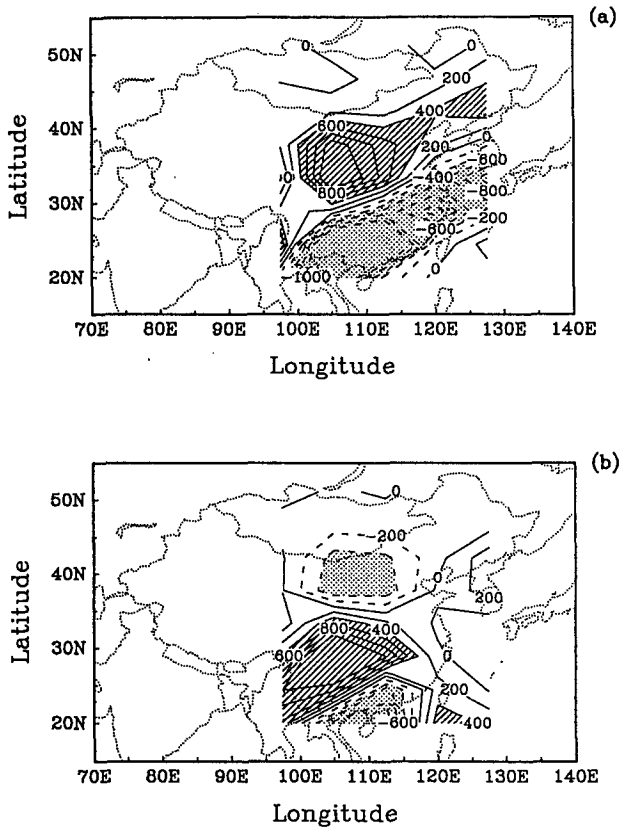

FIG. 4. Same as Fig. 3 except that the EOFs are developed with simulated rainfall anomaly data for model years 1–40.

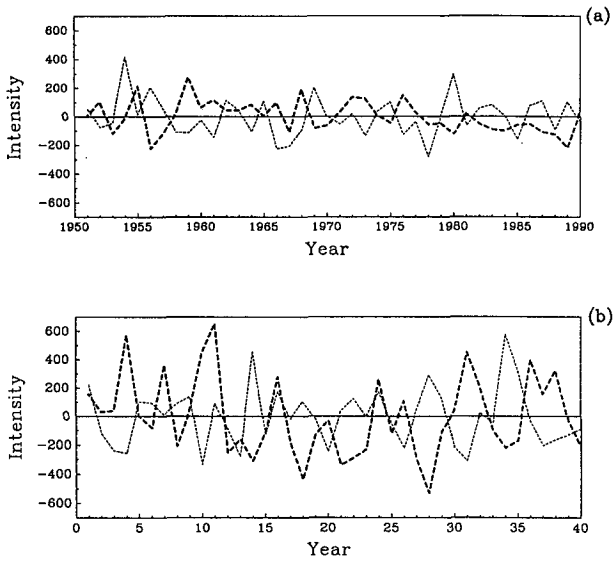

FIG. 5. Regional intensity index time series for the Yangtze River valley (dotted line) and southeast China (dashed line) for 1951–1990 (a) and model years 1–40 (b).

EOF analysis is also applied to the model summer rainfall anomaly dataset to identify GCM rainfall regions over China. The loading pattern of simulated EOF1 (Fig. 4a) is similar to that of observed EOF2 (Fig. 3b) and indicates that the Yangtze River valley is the boundary between centers to the north and south. Simulated EOF2 (Fig. 4b) is comparable to observed EOF1 (Fig. 3a), where loading centers are located over the Yangtze River valley and southeast China. A third, well-defined loading center is generated over northeast China. Total GCM rainfall anomaly variance explained by EOF1 and EOF2, 22.6% and 11.7%, is substantially more than the observed values. The simulated loading patterns again indicate rainfall regions over the Yangtze River valley and southeast China (Table 1). The GCM region locations, however, are systematically shifted approximately one grid cell to the west (i.e., 7.5° long). Note that, relative to observations, the axis of GCM loadings has a greater southwest to northeast tilt. In addition, the model loadings are much larger than observed values. This occurs because anomaly interannual variability in the GCM rainfall regions is much larger than that in the observed regions (shown below).

For each observed and GCM rainfall region, an intensity index is developed in order to provide a quantitative measure of anomaly interannual variability. Yearly summer rainfall for each observed region is defined by the average of 10 stations that are evenly distributed over the region. Anomalies are then given by differences between the annual averages and the 1951–1990 mean. The 40-yr anomaly time series for each region is defined to contain a set of annual intensity index values. For each GCM region, summer rainfall is defined by a four grid cell area that corresponds to the locations of the largest EOF loadings. Regional rainfall for a specific summer is given by the four grid cell average, whereas the anomaly is the difference between that average and the mean for years 1–40. The resulting anomaly time series for each region is defined to contain a set of GCM intensity index values. An analysis of the intensity index time series for each rainfall region (Fig. 5) indicates that the standard deviation of GCM generated precipitation is larger than that for observations (Table 2).

Relationships between the intensity indices and the Eurasian sea level circulation are determined to identify the physical mechanisms that explain regional rainfall interannual variability. Single point correlations between sea level pressure anomalies and each intensity

TABLE 2. Summer anomaly standard deviations (in millimeters) over each observed and GCM rainfall region.

Region	Observed SD	GCM SD
Yangtze River valley	137.6	202.9
Southeast China	111.3	277.3

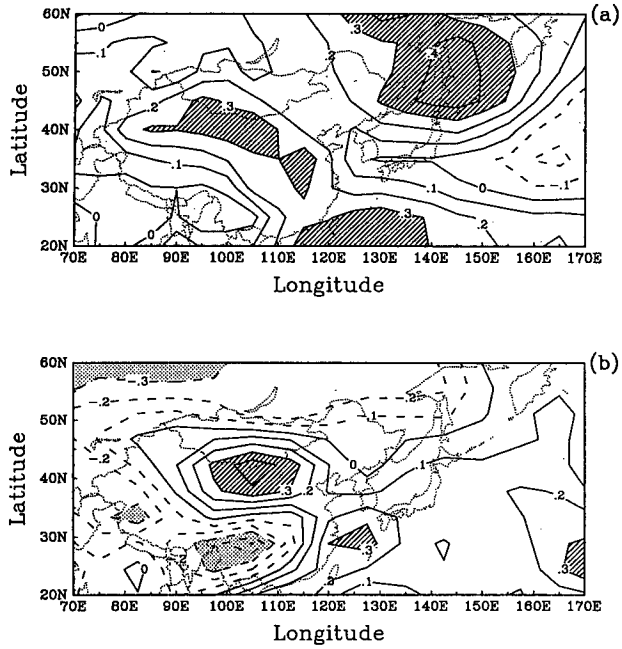

FIG. 6. Spatial distribution of correlation coefficients between the Yangtze River valley intensity indices and summer sea level pressure for observations (a) and the GCM. Contour interval is 0.1. Hatched areas correspond to coefficients greater than +0.30, while stippling indicates values less than −0.30.

index time series are calculated. Coefficient values are then mapped and analyzed. A correlation is statistically significant at the 95% level when the coefficient magnitude is greater than 0.31. Hereafter, all relationships between regional intensity and the sea level circulation will be discussed in terms of increasing intensity.

There are three areas of significant positive correlations between observed Yangtze River valley rainfall intensity and sea level pressure (Fig. 6a). The first is located over a region of the Pacific Ocean that is adjacent to the southeast China coast, the second occurs along an axis that reaches from northwest China to the Yangtze River valley, and the third extends from southeast Siberia to the Kamchatka Peninsula. The correlation pattern indicates that increased precipitation along the Yangtze River valley occurs in response to changes in the strength of the Siberian high and the location of the subtropical high. As the Siberian high becomes stronger and the subtropical high ridges toward the east China coast, the resulting circulation causes the thermal gradient across the Mei-Yu front to increase. The westward movement of the subtropical high also causes the longitudinal pressure gradient over south China to increase. This results in enhanced southerly flow and moisture transport over the Yangtze River valley. Increased Yangtze River valley rainfall intensity is also identified with higher sea level pressure values over the Sea of Okhotsk. Tao and Chen (1987) found that the blocking Okhotsk high becomes established when heavy summer rainfall occurs along the Yangtze River valley. During these years, transient disturbances on the south side of the Okhotsk high advect cold air over the Yangtze River valley and enhance the temperature gradient across the Mei-Yu front.

Significant positive correlations between GCM intensity over the Yangtze River valley and simulated sea level pressure (Fig. 6b) occur over north-central China and along the east China coast while large negative coefficients are located over south-central China. The coefficient pattern indicates that Yangtze River valley rainfall intensifies when both the Siberian high and the monsoon low strengthen and the subtropical high ridges toward the east China coast. As is the case in observations, the circulation associated with the Siberian and subtropical highs causes the temperature gradient along the Mei-Yu front to increase. Furthermore, an enhanced east–west pressure gradient over the southern half of China again causes the southerly wind component and moisture transport to increase over the Yangtze River valley. Coefficient values over the Sea of Okhotsk, however, are close to zero. In addition, the negative correlation between GCM intensity over the Yangtze River valley and the monsoon low is much larger than that found in observations (Fig. 6a).

Correlations between observed southeast China rainfall intensity and sea level pressure (Fig. 7a) are negative over virtually all of Eurasia. Coefficient values are significantly less than zero along an axis that extends

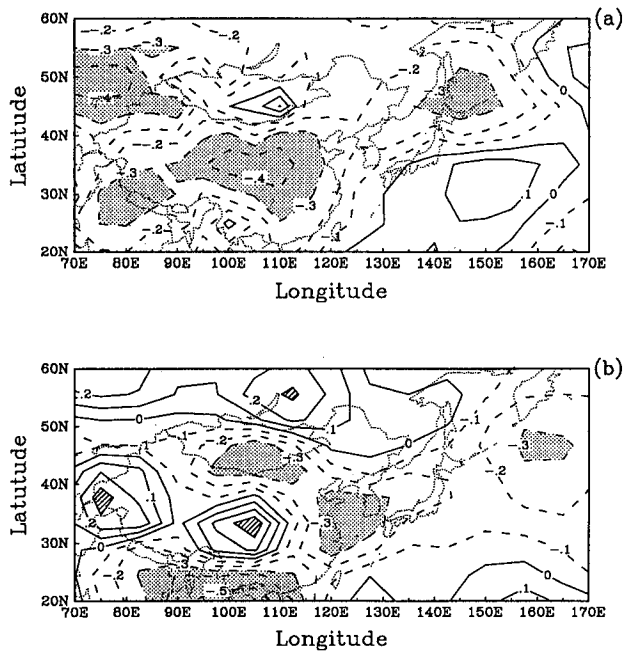

FIG. 7. Same as Fig. 6 except that correlations are calculated with southeast China intensity indices.

from northern India to northern Japan. Additional significant negative correlations are located over southwest Siberia. Small positive correlations occur over the west-central Pacific Ocean. The coefficient pattern indicates that summer rainfall intensifies over southeast China when the monsoon low migrates to the north and east of its mean position. This causes the zonal pressure gradient, southerly wind component, and moisture transport to increase across southeast China.

Large negative correlations between GCM intensity over southeast China and simulated sea level pressure (Fig. 7b) are located over the northeast China coast, Mongolia, and an area that extends from east India to the south China coast. Coefficient values are significantly greater than zero over the Tibetan Plateau. In contrast with observations, the correlation pattern indicates that GCM rainfall intensity over southeast China increases when sea level pressure rises on the north side of the monsoon low and falls to the south and east of the low center. This change in the configuration of the monsoon low causes southwesterly flow and moisture transport to increase over southeast China.

Finally, in order to verify the results of the correlation analysis, sea level pressure anomaly composite fields are calculated for sets of years when the magnitude of observed and GCM rainfall over the Yangtze River valley and southeast China is more than one standard deviation above the mean values. The resulting maps (not shown) indicate that the locations of the largest anomalies correspond closely to those of the correlation coefficient centers in Figs. 6 and 7.

4. Conclusions

The East Asian summer monsoon is described in terms of rainfall over China and the Eurasian sea level circulation. We then compare observed monsoon characteristics with those in a GCM simulation of the present climate.

EOF analysis is used to determine the specific locations of rainfall regions in China, where anomaly interannual variability is large but relatively homogeneous. The EOF loading patterns indicate that rainfall regions in both observations and the model simulation are found over the Yangtze River valley and southeast China, where the GCM regions are located several degrees to the west. An intensity index time series, based on area-averaged summer rainfall, is then developed for each observed and GCM region in order to quantify anomaly interannual variability.

Single-point correlations between the intensity indices and gridded sea level pressure are calculated, mapped, and analyzed to identify physical mechanisms that explain anomaly interannual variability in the observed and GCM rainfall regions. The coefficient patterns indicate that several sea level circulation features interact to influence regional rainfall intensity. Specifically, observed Yangtze River valley rainfall intensifies when the Siberian high strengthens and the subtropical high ridges toward the east China coast. These features cause the meridional temperature gradient, southerly wind flow, and moisture transport across the Mei-Yu front to increase. Intensified Yangtze River valley rainfall is also linked to higher sea level pressures over the Sea of Okhotsk. Tao and Chen (1987) showed that transient disturbances on the south side of the Okhotsk high advect cold air over the Yangtze River valley and increase the temperature gradient across the Mei-Yu front. The GCM accurately reproduces observed interactions between the monsoon low and subtropical high that lead to enhanced rainfall over the Yangtze River valley. The increase in sea level pressure over the Sea of Okhotsk, however, is not simulated. Observed intensity over southeast China increases when the monsoon low moves to the north of its mean position and the subtropical high ridges toward the east China coast. In contrast, GCM intensity is greater when the monsoon low deepens over southeast China and sea level pressures rise over the Tibetan Plateau. In both observations and the simulation, the southerly component of the wind and moisture transport increase over southeast China.

Although the formulation of the GCM used in this study has unrealistic topography and does not generate sufficient interannual variability in tropical sea surface temperatures, our results indicate that the model does reproduce specific features of the observed east Asian summer monsoon. These include rainfall region locations in China as well as physical relationships between regional rainfall intensity over the Yangtze River valley and the Eurasian sea level circulation. Future study will focus on the ability of GCMs with finer horizontal grid resolutions and coupled atmosphere–ocean models to reproduce observed east Asian summer monsoon characteristics. As a part of this research, the monsoon must be described in greater detail to compensate for the smaller spatial and temporal scales that the higher-resolution models are able to simulate.

Acknowledgments. The authors wish to thank Drs. Qiap-Yun Zhang and Xin-Zhong Liang for their instructive comments and suggestions. This research was supported by the Environmental Sciences Division, Office of Health and Environmental Research, Department of Energy.

REFERENCES

Fu, C.-B., H. F. Diaz, and J. O. Fletcher, 1986: Characteristics of response of sea surface temperature in the central Pacific associated with warm episodes of the Southern Oscillation. *Mon. Wea. Rev.*, **114**, 1716–1738.

Giorgi, F., 1990: Simulation of regional climate using a limited area model nested in a general circulation model. *J. Climate*, **3**, 941–963.

Hurrell, J. W., J. J. Hack, and D. P. Baumhefner, 1993: Comparison of NCAR Community Climate Model (CCM) climates. National

Center for Atmospheric Research Tech. Note, NCAR/TN-395+STR, 335 pp.

Jenne, R., 1989: Data availability at NCAR (selected datasets). National Center for Atmospheric Research Tech. Note, NCAR TN/IA-111, 45 pp.

Lau, K.-M., and M. T. Li, 1984: The monsoon of east Asia and its global associations-a survey. *Bull. Amer. Meteor. Soc.*, **65,** 114–125.

——, G. J. Yang, and S. H. Shen, 1988: Seasonal and intraseasonal climatology of summer monsoon rainfall over east Asia. *Mon. Wea. Rev.*, **116,** 18–37.

Legates, D. R., and C. J. Wilmott, 1990: Mean seasonal and spatial variability in gauge-corrected global precipitation. *Int. J. Climatol.*, **10,** 111–128.

Liang, X.-Z., A. N. Samel, and W.-C. Wang, 1995a: Observed and GCM simulated decadal variability of monsoon rainfall in China. *Climate Dyn.*, in press.

——, W.-C. Wang, and M. P. Dudek, 1995b: Interannual variability of regional climate and its change due to the greenhouse effect. *Global and Planet. Change,* in press.

Sperber, K. R., S. Hameed, G. L. Potter, and J. S. Boyle, 1994: Simulation of the northern summer monsoon in the ECMWF model: Sensitivity to horizontal resolution. *Mon. Wea. Rev.*, **122,** 2461–2481.

Tao, S., and L. Chen, 1987: A review of recent research on the east Asian summer monsoon in China. *Monsoon Meteorology,* T. N. Krishnamurti, Ed., Oxford University Press, 60–92.

——, C. Fu, Z. Zeng, and Q.-Y. Zhang, 1991: Two long-term instrumental climate data bases of The Peoples Republic of China. Environmental Sciences Division, DOE, Publication No. 3747, ORNL/CDIAC-47, NDP-039, 83 pp.

Tibaldi, S., T. N. Palmer, C. Brankovic, and U. Cubasch, 1990: Extended range predictions with ECMWF models: Influence of horizontal resolution on systematic error and forecast skill. *Quart. J. Roy. Meteor. Soc.*, **116,** 835–866.

——, and K. Li, 1990: Precipitation fluctuation over semiarid region in northern China and the relationship with El Niño/Southern Oscillation. *J. Climate,* **3,** 769–783.

——, M. P. Dudek, and X.-Z. Liang, 1992: Inadequacy of effective CO_2 as a proxy in assessing the regional climate change due to other radiatively active gases. *Geophys. Res. Lett.*, **19,** 1375–1378.

Zhu, B., and D. Li, 1992: The relationship between tropical Pacific sea surface temperature and summer rainfall over northwest China. *Acta Meteor. Sinica,* **6,** 470–478.